

# Charge compensation analysis of Li-rich layered oxide positive electrode using X-ray absorption fine structure measurement in the soft X-ray region

Keisuke Yamanaka<sup>1</sup>, Masatsugu Oishi<sup>2</sup>, Koji Nakanishi<sup>1,2</sup>,  
Iwao Watanabe<sup>1,2</sup>, Toshiaki Ohta<sup>1</sup>

<sup>1</sup>SR Center, Ritsumeikan University, Kusatsu, Shiga 525-8577, Japan

<sup>2</sup>Office of Society-Academia Collaboration for Innovation, Kyoto University, Gokasho, Uji, Kyoto 611-0011, Japan

E-mail: k-yamana@fc.ritsumei.ac.jp

## Abstract

O K-edge and Mn L<sub>2,3</sub>-edge XAFS spectra of charged/discharged Li<sub>2</sub>MnO<sub>3</sub> positive electrodes were observed to reveal the charge compensation mechanism of Li-rich layered oxides as LIB positive electrode materials. In the charge/discharge measurements, the profile at the first charge process was quite different from that after the first discharge. This result suggests that only the electrochemical reaction at the first charge process is different from any other process. O K-edge and Mn L<sub>2,3</sub>-edge XAFS spectra at each charge/discharge reaction on the Li<sub>2</sub>MnO<sub>3</sub> positive electrode. These XAFS results suggest that the charge compensations are achieved by oxygen desorption from the Li<sub>2</sub>MnO<sub>3</sub> active material in the first charge process, and by the redox reaction of Mn at the lower voltage and O at the higher voltage after the first discharge.

## 1. Introduction

Lithium ion secondary battery (LIB) is one of a high performance energy storage system and used for some mobile devices instead of lead storage battery and nickel-hydrogen battery and so on. The use of LIB was extended such as hybrid electric vehicle (HEV) and smart grid for household use in the recent year, additionally to improve the performance of LIB is expected for practical electric vehicle (EV) and smart grid electricity network system in the future. Layered transition metal oxides such as  $\text{LiCoO}_2$  [and olivine type  $\text{LiFePO}_4$  is conventional positive electrode material for LIB. Their practical capacity is around 150mAh/g that is insufficient for the future application. Thus, it is very important to understand the electrochemical reaction of LIB in more detail for further development of LIB performance.

Non-destructive X-ray analysis was widely used for LIB analysis. Among them, X-ray Absorption Fine Structure (XAFS) is element-selective and sensitive to the formal oxidation state, coordination chemistry, and the distances. Thus, XAFS is very powerful tool to investigate the charge compensation mechanism, and degradation mechanism of LIB cell. One of the typical applications of XAFS for LIB is redox reaction analysis of transition metal in cathode active material using hard X-ray. According to that, it was proved that Co is oxidized/reduced with Li extraction/insertion in  $\text{LiCoO}_2$  [1], in addition, Fe is oxidized/reduced with Li extraction/insertion in  $\text{LiFePO}_4$  [2]. In recent years, hard X-ray XAFS measurements without disassembling the LIB cell, namely, 'in-situ' XAFS measurements are becoming general and widely utilized.

In order to enhance the power density of LIB, it might be required to increase the Li content in cathode, to raise the potential vs  $\text{Li/Li}^+$ , and so on. Li-rich layered oxide cathode material recently attracts attention as high capacity cathode material.  $\text{Li}_2\text{MnO}_3$ , that is one of the typical material of Li-rich layered oxide, possesses high theoretical capacity of 459mAh/g. The capacity of 300mAh/g was actually observed in the first charge process in  $\text{Li}_2\text{MnO}_3/\text{Li}$  cell [5]. However,  $\text{Li}_2\text{MnO}_3$  is not practical because of its poor coulombic efficiency especially in the first cycle. Thus,  $\text{Li}_2\text{MnO}_3\text{-LiMO}_2$  ( $M=\text{Mn, Co, Ni}$ ) system was proposed as Li-rich layered oxide that has excellent cycleability and high capacity of 300mAh/g [6-9].

The features of Li-rich layered oxide are not only high Li content but also its charge compensation mechanism in the charge/discharge process. In the conventional cathode material such as  $\text{LiCoO}_2$ , as mentioned above, Co is oxidized/reduced during the charge/discharge. In contrast, it was revealed that the valence state of Mn is unchanged during the first charge in  $\text{Li}_2\text{MnO}_3$  electrode in the previous studies [8]. Thus, oxygen contribution to the charge compensation is expected in  $\text{Li}_2\text{MnO}_3$  electrode. Oxygen contribution to the charge compensation might be very important for developing the power density of LIB because of its

high potential vs Li/Li<sup>+</sup>. However, details of the charge compensation mechanism of Li<sub>2</sub>MnO<sub>3</sub> is not understood sufficiently now.

In this study, O K-edge and Mn L<sub>2,3</sub>-edge XAFS measurements using soft X-ray were carried out to investigate details of the charge compensation mechanism of Li<sub>2</sub>MnO<sub>3</sub> electrode. In addition, some analysis methods valid for LiB analysis will be also introduced below.

## 2. Experimental Methods

### 2.1 Preparation of Li<sub>2</sub>MnO<sub>3</sub> positive electrode

Li<sub>2</sub>MnO<sub>3</sub> powder was prepared by solid state reaction between LiOH · H<sub>2</sub>O and MnCO<sub>3</sub>. Each starting material was mixed by ball milling so that the molar ratio of Li and Mn is 2:1. The mixed powder is pelletized and calcinated at 973K in the air for 24h. The obtained active material was mixed with conducting assistant (acetylene black) and binder (Poly Vinylidene DiFluoride) so that their weight ratio is 8:1:1 and spread onto aluminum foil by NMP (N-MethylPyrrolidone). The foil was dried and pressed to make mixing electrode. Finally, LIB cell composed of Li<sub>2</sub>MnO<sub>3</sub> mixing electrode (positive electrode), lithium metal (negative electrode), separator, and electrolyte (1M-LiPF<sub>6</sub>, EC:DEC=3:7) was assembled in the globe box filled by dry argon gas.

Electrochemical measurement was carried out in the thermostatic chamber kept at 25°C. Charge/discharge measurements were performed in the potential range of 2.0V-4.8V at current rate of 0.05C. After the charge/discharge test, Li<sub>2</sub>MnO<sub>3</sub> electrode was extracted from Li<sub>2</sub>MnO<sub>3</sub>/Li cell and washed by DMC (DiMethyl Carbonate) in the glove box. In addition, Li<sub>2</sub>MnO<sub>3</sub> electrode extracted from Li<sub>2</sub>MnO<sub>3</sub>/Li cell after soaking in electrolyte (named 'Initial') was prepared by the same way as the electrode sample before charging.

The prepared samples were mounted on the sample holder by carbon tape and stored in the transfer vessel our group developed [10] under Ar atmosphere. The transfer vessel was installed in the load-lock chamber at BL-11 of Ritsumeikan SR center (Fig.1) without air exposure.

### 2.2 Soft X-ray absorption measurements

XAFS measurement at Oxygen K-edge and Mn L<sub>2,3</sub>-edge were carried out at BL-11 of Ritsumeikan SR center. In this beamline, three varied line-spacing plane gratings that supply monochromatized photon beam with  $h\nu=40-1000$  are employed. Sample chamber (Fig.1) was in ultra-high vacuum condition ( $\sim 1 \times 10^{-6}$  Pa) for soft X-ray XAFS measurement. XAFS measurement geometry is shown in Fig.2. As shown in Fig.2, XAFS spectra were taken simultaneously in TEY (Total Electron Yield) mode and PFY (Partial Fluorescence

Yield) mode. TEY mode that detects secondary electron by drain current method is surface sensitive detection method. On the other hand, PFY mode that detects fluorescence by silicon drift detector (SDD) with polyethylene window (100nm thickness) is bulk sensitive detection method [11]. Additionally, IPFY (Inverse Partial Fluorescence Yield) mode that is called self-absorption free method was used at Mn  $L_{2,3}$ -edge instead of PFY mode, because the XAFS signal at Mn  $L_{2,3}$ -edge is distorted by self-absorption effect in PFY mode [12,13].

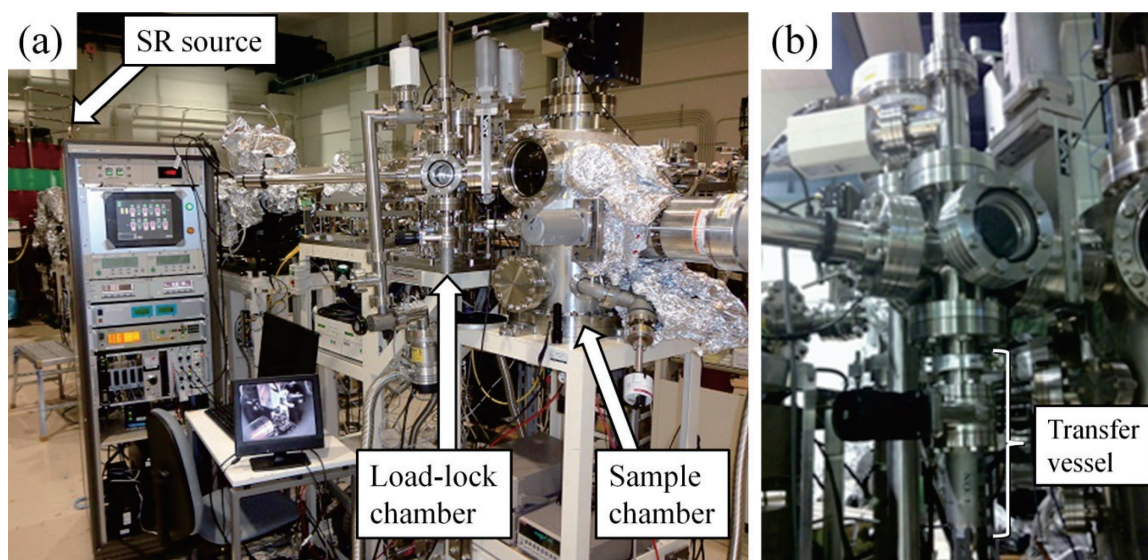


Fig.1 Photos of the BL11 at the SR center, Ritsumeikan University. (a) The SR source and BL11. (b) The load lock chamber with the transfer vessel.

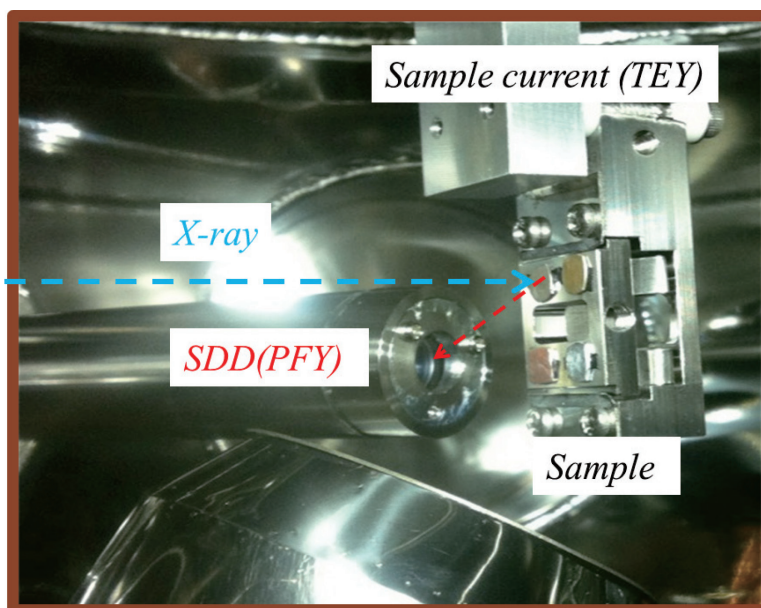


Fig.2 XAFS measurement geometry in BL-11

### 3. Results and discussion

#### 3.1 Electrochemical measurement

Charge/discharge profile of  $\text{Li}_2\text{MnO}_3/\text{Li}$  cell is shown in Fig.3. First charge and first discharge are represented '1c' and '1d', Second charge and second discharge are represented '2c' and '2d' respectively. The notation 'Initial' and '1-8' indicate as XAFS measurement point. In the first charging process, the characteristic voltage plateau was observed at 4.6V and the capacity at the cut-off voltage was 360mAh/g. In the first discharge process, on the other hand, the characteristic voltage plateau was not observed and the capacity drastically faded compare with the first charge. In the second charge/discharge process, the characteristic voltage plateau was not observed too. These features of charge/discharge profile were same as the previous study.

It was suggested that the characteristic voltage plateau at 4.6V is caused by oxygen desorption from  $\text{Li}_2\text{MnO}_3$  in the previous study[3]. The charge compensation analysis in the first charge process using soft X-ray absorption will be shown below. Furthermore, the charge compensation after the oxygen desorption will be discussed.

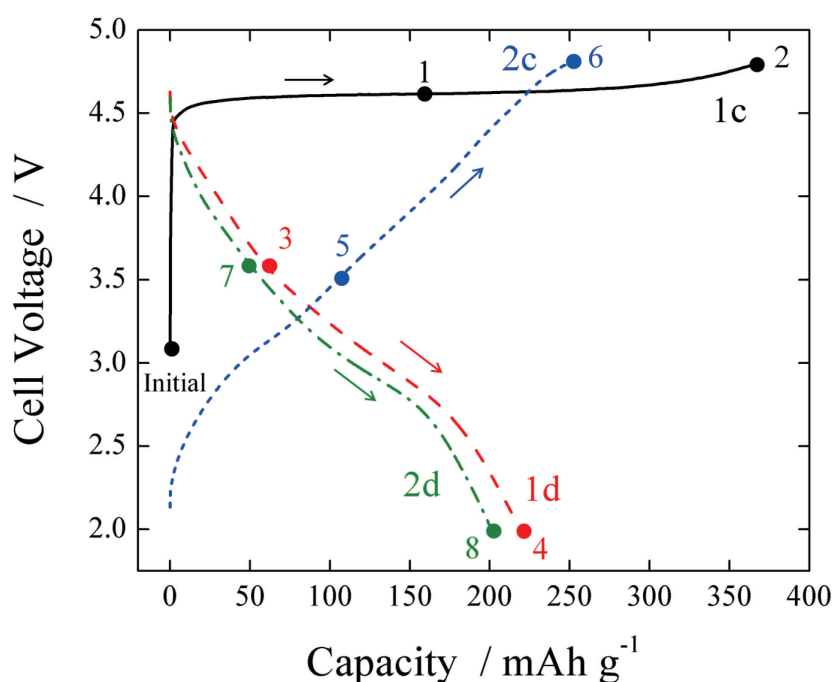


Fig.3 Charge/discharge profile of  $\text{Li}_2\text{MnO}_3$  cathode at the first charge process ('1c'), first discharge process ('1d'), second charge process ('2c'), and second charge process ('2d'). The notations: 'Initial' and '1-8' indicate as XAFS measurement points.

#### 3.2 Charge compensation mechanism in the first charge process

O K-edge and Mn  $L_{2,3}$ -edge XAFS measurements of 'Initial' and '1-2' were carried out to investigate the charge compensation mechanism in the first charge process. Mn  $L_{2,3}$ -edge

XAFS spectra are shown in Fig.4. XAFS spectra of MnO, Mn<sub>2</sub>O<sub>3</sub>, and Li<sub>2</sub>MnO<sub>3</sub> powder are put on Fig.4 as reference spectra of Mn<sup>2+</sup>, Mn<sup>3+</sup>, and Mn<sup>4+</sup>. First, the chemical state of Mn before charge was tetravalent because the XAFS spectrum of ‘initial’ corresponded with that of Li<sub>2</sub>MnO<sub>3</sub> powder. Subsequently, there was no clear difference between XAFS spectrum of ‘Initial’ and that of ‘1-2’. These results prove that Mn does not contribute to the charge compensation in the first charge process. Besides, a very small peak shift was observed at Mn L<sub>2</sub>-edge in XAFS spectra of charged sample. The reason of this extraordinary behavior will be discussed later.

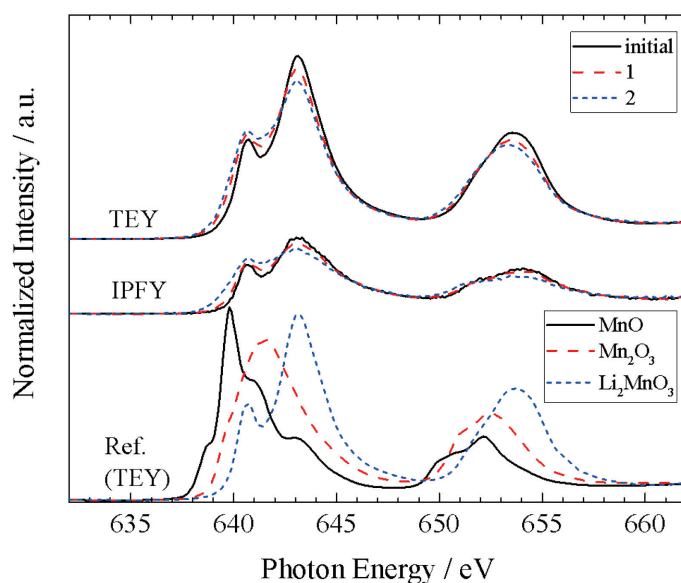


Fig.4 Observed Mn L<sub>2,3</sub>-edge XAFS spectra at each charge depth (‘Initial’, ‘1’, and ‘2’ which are labeled in Fig.3) in the first charge process using the TEY and IPFY modes, and observed reference samples (‘Ref.’) using the TEY mode.

O K-edge XAFS spectra are shown in Fig.5. O K-edge XAFS spectra of transition metal oxide consist of two spectrum region. One is the broad structure observed above 535eV, in addition another is the sharp structure at the pre-edge region. Former region attribute to oxygen *p* character hybridized with *4s* and *4p* states of transition metal. The broad structure is called ‘shape resonance’, that reflects local structure of oxygen around transition metal [14]. On the other hand, latter region attribute to oxygen *p* character hybridized with *3d* states of transition metal. The pre-edge structure is sensitive to the valence state of oxygen and transition metal. In particular, the pre-edge peak position relate to the effective nuclear charge of transition metal, in addition, pre-edge peak intensity is proportional to Oxygen *2p* hole

number [14]. O K-edge XAFS spectrum of ‘initial’ has three peaks in the pre-edge region, observed at 529eV, 531eV, and 533eV. Their assignments are considered as the transition from O  $1s$  to  $t_{2g}$  (O  $2p$  hybridized with Mn  $3d$ ),  $e_g$  (O  $2p$  hybridized with Mn  $3d$ ), and  $\pi^*$ (C=O bond of carbonate) respectively. The intensity of the first peak (assigned as the transition from O  $1s$  to  $t_{2g}$ ) slightly decreased after the first charge, namely, after lithium extraction. If oxygen contributes to the charge compensation in the first charge process, oxygen  $2p$  hole and the intensity of first peak must increase. Consequently, it was proved that lattice oxygen in  $\text{Li}_2\text{MnO}_3$  does not contribute the charge compensation in the first charge process too.

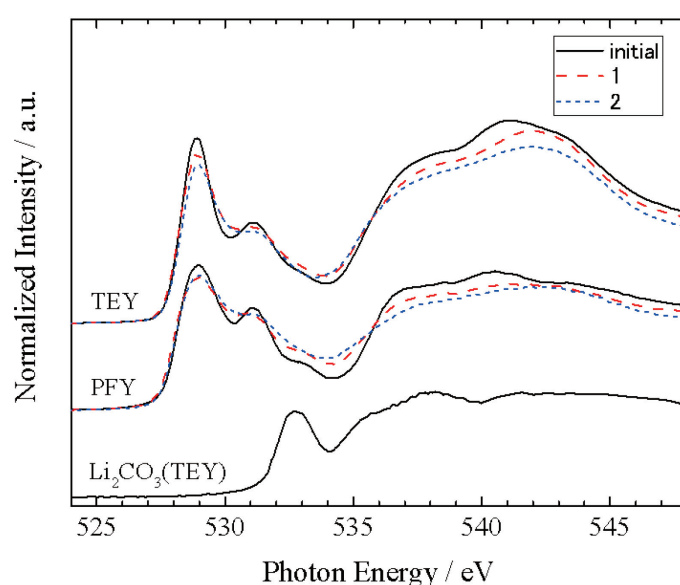


Fig.5 Observed O K-edge XAFS spectra at each charge depth (‘Initial’, ‘1’, and ‘2’ which are labeled in Fig.3) in the first charge process using the TEY and PFY modes, and  $\text{Li}_2\text{CO}_3$  powder as a reference using the TEY mode.

These XAFS results suggest that the charge compensation occurs by oxygen desorption as the previous studies suggested [3]. The evaluation of oxygen desorption by the edge-jump analysis of O K-edge and Mn L-edge XAFS was carried out (Fig.6). The edge jump height of absorption edge is proportional to amount of the element, so edge jump ratio of O K-edge and Mn L-edge is equivalent to the composition ratio of O and Mn. Fig.6 (a) shows wide range absorption spectra including O K-edge and Mn L-edge. These spectra were normalized at O K-edge jump, so Mn L-edge jump height change during first charge shows the change of composition ratio of O and Mn. Although there is no Mn source, Mn L-edge jump height

increase as the charging capacity increase. This results suggest that the change of composition ratio of O and Mn caused by oxygen desorption in the first charge process. Fig.6 (b) shows the edge jump height ratio of O K and Mn L absorption edge as a function of charging capacity. In the first charge process, the composition ratio of O and Mn is completely proportional to charging capacity. Consequently, it is conceivable that the charge compensation mechanism in the first charge process can be explained by oxygen desorption.

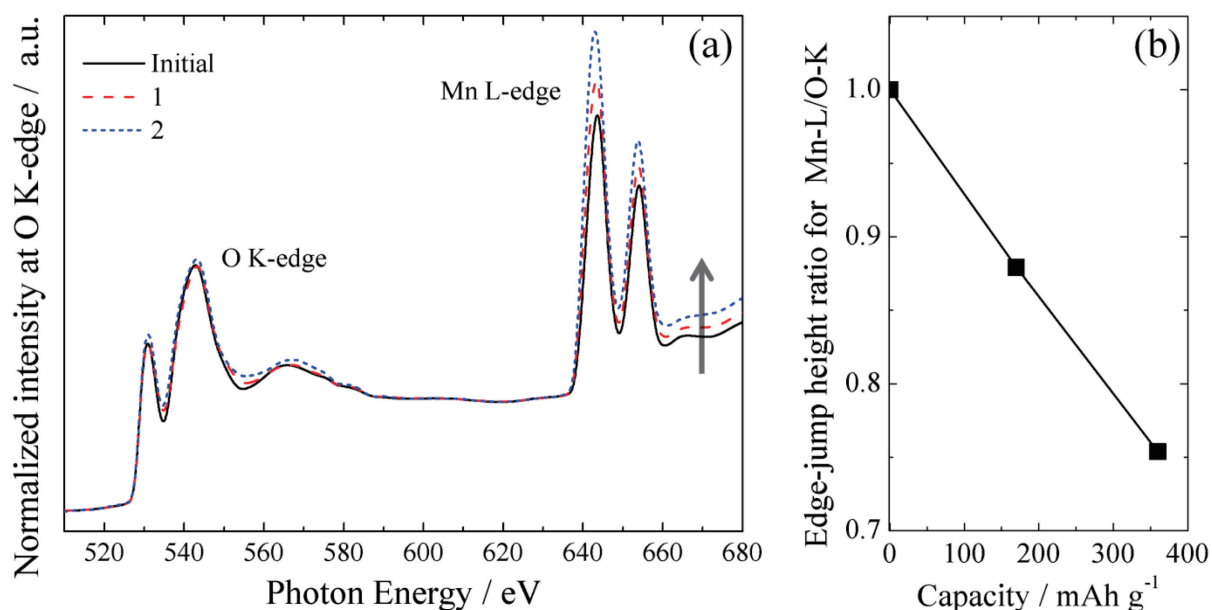


Fig.6 Comparison among XAFS spectral edge-jump heights using the TEY mode at each charge depth ('Initial', '1', and '2' which are labeled in Fig.3) in the first charge process. (a) Comparison among Mn L-edge XAFS spectra based on normalized O K-edge XAFS. (b) Plotted Mn L-edge (Mn-L) jump heights v.s. O K-edge (O-K) jump heights.

### 3.3 Charge compensation mechanism after the first charge

The charge/discharge profile of Li<sub>2</sub>MnO<sub>3</sub>/Li cell shows the characteristic voltage plateau at 4.6V in the first charge, and the gradual curve with small voltage plateau around 3.0V after the first charge. It is suggested that the charge compensation mechanism after the first charge is quite different from that in the first charge process. Then, O K-edge and Mn L<sub>2,3</sub>-edge XAFS measurements of '3-8' were carried out to investigate the charge compensation mechanism after the first charge.

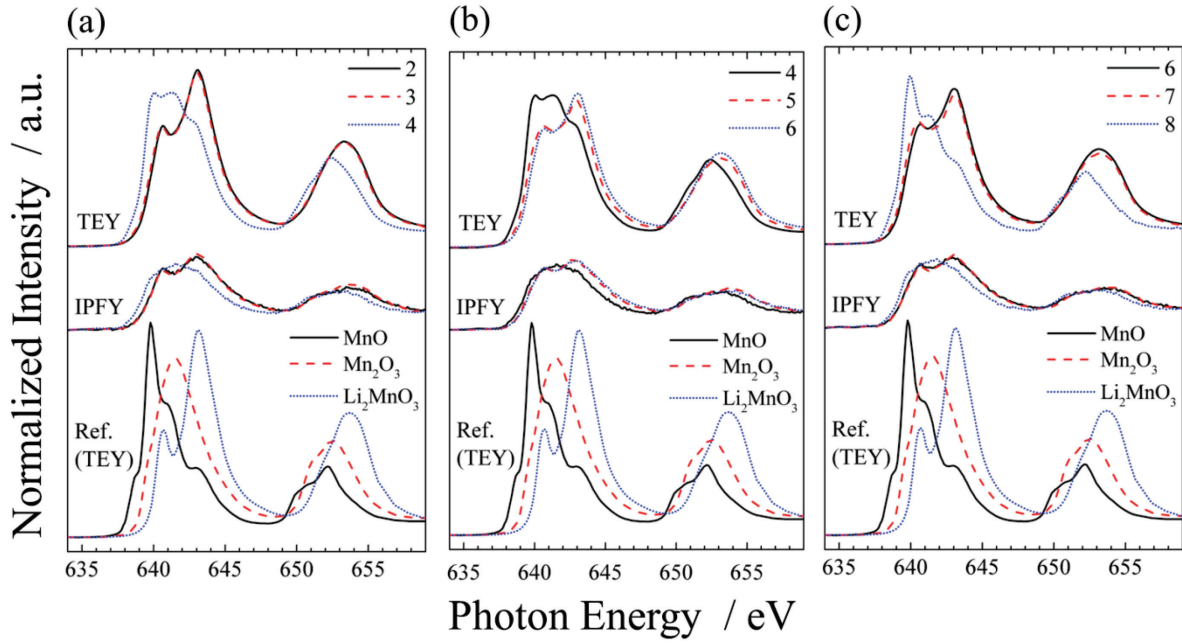


Fig.7 Observed Mn  $L_{2,3}$ -edge XAFS spectra at each charge/discharge depth using the TEY and IPFY modes, and observed reference samples ('Ref.') using the TEY mode. (a) First discharge process ('2', '3', and '4' which are labeled in Fig.3). (b) Second charge process ('4', '5', and '6' which are labeled in Fig.3). (c) Second discharge ('6', '7', and '8' which are labeled in Fig.2).

Mn  $L_{2,3}$ -edge XAFS spectra of '2-4' are shown in Fig.7 (a). The spectrum change between them shows the chemical state change of Mn in the first discharge process. As Fig.3 shows, the chemical state of Mn after first charge, that is sample '2', is almost tetravalent. There was no clear difference between the XAFS spectrum of '2' and that of '3'. In contrast, XAFS spectrum of fully discharged sample '4' is drastically different from that of '3'. The drastic change of XAFS spectra is considered as increasing  $Mn^{2+}$  and  $Mn^{3+}$  components during the small voltage plateau around 3.0V. Mn  $L_{2,3}$ -edge XAFS spectra of samples in the second charge and discharge process are shown in Fig.7 (b) and (c) respectively. XAFS spectrum of '5' that is charged through the small voltage plateau around 3.0V was drastically different from that of '4'. This change is considered as increasing  $Mn^{4+}$  and decreasing  $Mn^{2+}$  and  $Mn^{3+}$ . Subsequently, there was no clear difference between XAFS spectrum of '5' and that of '6' same as the first discharge process. This behavior was observed in second discharge process too. Consequently, Mn contributes to the charge compensation in the charge/discharge process by oxidation/reduction occurs at small voltage plateau around 3.0V. In the high voltage region, oxygen contribution to the charge compensation is expected.

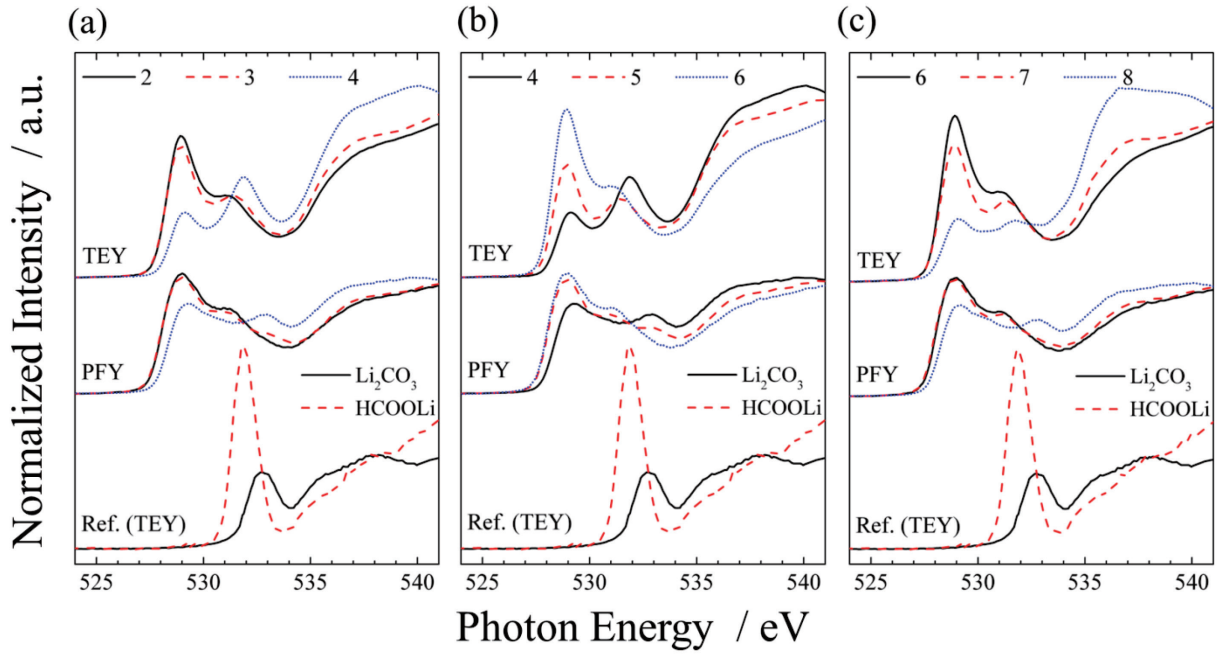


Fig.8 Observed O K-edge XAFS spectra at each charge/discharge depth using the TEY and PFY modes, and observed reference samples ('Ref.') using the TEY mode. (a) First discharge process ('2', '3', and '4' which are labeled in Fig.3). (b) Second charge process ('4', '5', and '6' which are labeled in Fig.3). (c) Second discharge ('6', '7', and '8' which are labeled in Fig.2).

O K-edge XAFS spectra of '2-4' are shown in Fig.8 (a). Although the charge compensation by oxygen is expected, the difference between XAFS spectrum of '2' and that of '3' was very small. The detail will be discussed later. In contrast, the intensity of first peak drastically decreased after fully discharged because of oxygen  $2p$  hole annihilation by Mn reduction [14]. O K-edge XAFS spectra of samples in the second charge and discharge process are shown in Fig.8 (b) and (c) respectively. Similarly, decreasing the first peak intensity occurred during the small voltage plateau around 3.0V in the second charge and discharge process. In addition, the change of O K-edge XAFS spectra were very small too during the high voltage region. More detail analysis is necessary in order to reveal the oxygen contribution to charge compensation in the high voltage region. As mentioned above, the intensity of pre-edge peak reflects the number of oxygen  $2p$  hole. Therefore, oxygen contribution to charge compensation can be revealed by pre-edge intensity analysis of O K-edge XAFS spectra. However, there were extra species, that is carbonyl or carbonate, in O K-edge XAFS spectra. In this study, pre-edge intensity analysis was carried out using only PFY spectra removed the extra species. In order to remove the extra species, the pre-edge region of O K-edge XAFS spectra was divided into  $t_{2g}$ ,  $e_g$ , and extra components by peak fitting. Gauss function and

arctangent function were used as each components and absorption edge, respectively. The result of pre-edge intensity analysis is shown in Fig.9. As mentioned above, the change of pre-edge intensity observed at small voltage plateau around 3.0V correspond to the oxidation/reduction of Mn. In contrast, although the chemical state of Mn was unchanged, pre-edge intensity increased/decreased at the high voltage region in charge/discharge process. Therefore, we believe that oxygen contributes to the charge compensation at the high voltage region. We speculate that the charge compensation at high voltage region occurs while keeping the valence of Mn by charge transfer from metal to oxygen because of the instability of high-valent Mn.

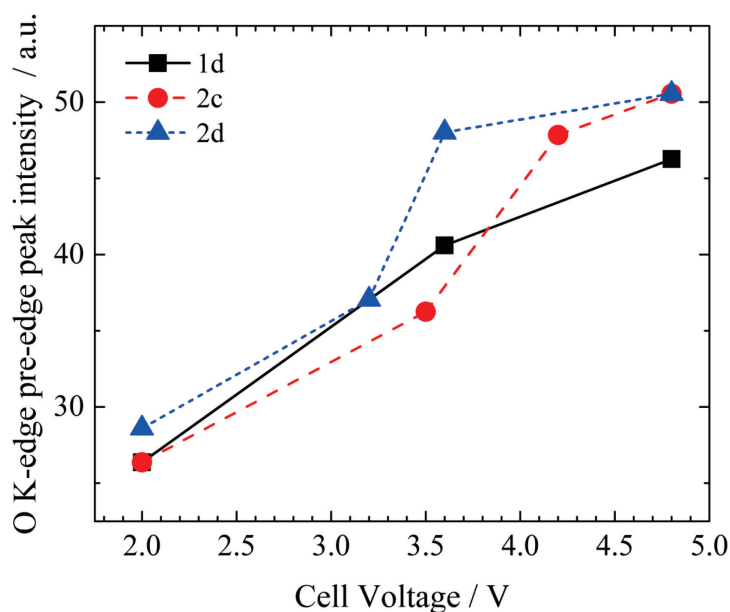


Fig.9 Plotted pre-edge intensities of O K-edge spectra using the PFY modes in the first discharge process ('1d'), second charge process ('2c'), and second charge process ('2d') in Fig.3.

#### 4. Conclusion

O K-edge and Mn  $L_{2,3}$ -edge XAFS measurements of  $\text{Li}_2\text{MnO}_3/\text{Li}$  cell were carried out in order to reveal the charge compensation mechanism of Li-rich layered oxide. It was proved that the charge compensation is achieved by oxygen desorption from  $\text{Li}_2\text{MnO}_3$  at the characteristic voltage plateau observed 4.6V in the first charge process. In contrast, the charge compensation is achieved by redox reaction of Mn at the lower voltage region, and O at the higher voltage region after the first charge.

As our study showed, soft X-ray absorption spectroscopy is very powerful for LIB analysis. In the future, that will be more important for the analysis of high capacity secondary battery using oxygen anion redox.

### Acknowledgements

This work was supported by Reserch and Development Initiative for Scientific Innovation of New Generation Batteries (RISING project).

### References

- [1] W.-S. Yoon, K-B. Kim: *J. Phys. Chem. B*, **106**, 2526-2532 (2002).
- [2] S. Yang, D. Wang, G. Liang, Y. M. Yiu, J. Wang, L. Liu, X. Sun, T-K. Sham: *Energy Environ. Sci.*, **5**, 7007 (2012).
- [3] K. Kubota, T. Kaneko, M. Hirayama, M. Yonemura, Y. Imanari, K. Nakane, R. Kanno: *J. Power Sources*, **216**, 249 (2012).
- [4] Z. Lue, J. R. Dahn: *J. Electrochem. Soc.*, **149**, A 815 (2002).
- [5] M. M. Thackeray, S.-H. Kang, C. S. Johnson, J. T. Vaughey, R. Benedek S. A. Hackney: *J. Mater. Chem.*, **17**, 3112 (2007).
- [6] N. Yabuuchi, K. Yoshii, S-T. Myung, I. Nakai, S. Komaba, *J. Am. Chem. Soc.*, **133**, 4404 (2011).
- [7] H. Koga, L. Croguennec, M. Menetrier, P. Manessiez, F. Weill, C. Delmas, S. Belin: *J. Phys. Chem. C*, **118**, 5700 (2014).
- [8] K. Kubobuchi, M. Mogi, H. Ikeno, I. Tanaka, H. Imai, T. Mizoguchi: *Appl. Phys. Lett.* **104**, 053906 (2014).
- [9] Y. Uchimoto, H. sawada, T. Yao: *J. Power Sources*, **97-98**, 326 (2001).
- [10] K. Nakanishi, T. Ohta: In “*Advanced Topics in Measurements*”, pp. 43 (2012), InTech, Croatia, ISBN: 978-953-51-0128-4.
- [11] C. Yogi, H. Ishii, K. Nakanishi, I. Watanabe, K. Kojima, T. Ohta, *Adv. X-ray. Chem. Anal. Japan* **43**, pp.147 (2012).
- [12] H. Wadati, A. J. Achkar, D. G. Hawthorn, T. Z. Regier, M. P. Singh, K. D. Truong, P. Fournier, G. Chen, T. Mizokawa, G. A. Sawatzky: *Appl. Phys. Lett.* **100**, 193906 (2012).
- [13] A. J. Achkar, T. Z. Regier, H. Wadati, Y.-J. Kim, H. Zhang, D. G. hawthorn, *Phys. Rev. B*, **83**, 081106 (2011).
- [14] F. M. F. de Groot, M. Grioni, J. C. Fuggle: *Phys. Rev. B*, **40**, 5715 (1989).